Published in final edited form as:

Cancer Res. 2023 April 04; 83(7): 1031–1047. doi:10.1158/0008-5472.CAN-22-2586.

Mutated HRAS activates YAP1-AXL signaling to drive metastasis of head and neck cancer

Sankar Jagadeeshan[1,2], **Manu Prasad**[1,2], **Mai Badarni**[1,2], **Talal Ben Lulu**[1,2], **Vijayasteltar Belsamma Liju**[1,2], **Sooraj Mathukkada**[1,2], **Claire Saunders**[1,2], **Avital Beeri Shnerb**[1,2], **Jonathan Zorea**[1,2], **Ksenia M Yegodayev**[1,2], **Monica Wainer**[1,2], **Liza Vtorov**[1,2], **Irit Allon**[2,3], **Ofir Cohen**[1,2], **Gro Gausdal**[4], **Dinorah Friedmann-Morvinski**[5,6], **Sok Ching Cheong**[7,8], **Alan L Ho**[9], **Ari J Rosenberg**[10], **Linda Kessler**[11], **Francis Burrows**[11], **Dexin Kong**[12], **Jennifer R Grandis**[13], **J Silvio Gutkind**[14], **Moshe Elkabets**[1,2]

[1]The Shraga Segal Department of Microbiology, Immunology, and Genetics, Ben-Gurion University of the Negev, Beer-Sheva, Israel.

[2]Faculty of Health Sciences, Ben-Gurion University of the Negev, Beer-Sheva, Israel.

[3]Institute of Pathology, Barzilai University Medical Center, Ashqelon, Israel.

[4]BerGenBio ASA, Bergen, Norway.

[5]School of Neurobiology, Biochemistry and Biophysics, The George S. Wise Faculty of Life Sciences, Tel Aviv University, Tel Aviv, Israel.

[6]Sagol School of Neuroscience, Department of Biochemistry and Molecular Biology, Tel Aviv University, Tel Aviv, Israel.

[7]Translational Cancer Biology, Cancer Research Malaysia, No. 1, Jalan SS12/1A, Subang Jaya, Selangor, Malaysia.

[8]Department of Oral and Maxillofacial Clinical Sciences, Faculty of Dentistry, University of Malaya, Kuala Lumpur, Malaysia.

[9]Memorial Sloan Kettering Cancer Center, New York, NY and Department of Medicine, Weill Cornell Medical College, New York City, NY, USA.

[10]Department of Medicine, Section of Hematology and Oncology, University of Chicago, Chicago, IL, USA.

[11]Kura Oncology, Inc., San Diego, CA, USA.

Correspondence: Prof. Moshe Elkabets, Faculty of Health Sciences, The Shraga Segal Department of Microbiology, Immunology, and Genetics, Ben-Gurion University of the Negev, Beer-Sheva 84105, Israel., moshee@bgu.ac.il.

Author contributions

Conceptualization: ME and SJ: Methodology: SJ, MP, MB, VBL, TBL, SM, CS, ABS, JZ, KMY, MW, LV, IA, DFM, DK and ME; Cell lines and Clinical sample: SCC, JRG and JSG; Drugs: GG provided R428, and LK and FB provided tipifarnib respectively; Writing—original draft: ME and SJ; Acquisition of data and critical revision of the manuscript: SJ, MP, MB, VBL, TBL, SM, DFM, DK, SCC, JRG, JSG, GG, LK, FB and ME: Supervision: ME. All authors read and approved the final manuscript.

Conflict of Interest

ME reported a grant from Kura Oncology.GG is an employee of BerGen Bio. JRG is the co-inventor of a decoy oligonucleotide targeting STAT3 that has been licensed by BluedotBio. JSG has received financial support from Kura Oncology, and he is consultant for io9, Domain Therapeutics, Pangea Therapeutics, and founder of Kadima pharmaceuticals, outside the submitted work. All others authors declare no conflicts of interest.

[12]School of Pharmaceutical Sciences, Tianjin Medical University, Tianjin, China.

[13]Department of Otolaryngology - Head and Neck Surgery, University of California San Francisco, San Francisco, CA, USA.

[14]Department of Pharmacology and Moores Cancer Center, University of California San Diego, La Jolla, CA, USA.

Abstract

The survival rate for head and neck cancer (HNC) patients diagnosed with cervical lymph node (cLN) or distant metastasis is low. Genomic alterations in the HRAS oncogene are associated with advanced tumor stage and metastasis in HNC. Elucidation of the molecular mechanisms by which mutated HRAS ($HRAS^{mut}$) facilitates HNC metastasis could lead to improved treatment options for patients. Here, we examined metastasis driven by mutant HRAS in vitro and in vivo using $HRAS^{mut}$ human HNC cell lines, patient-derived xenografts (PDXs), and a novel $HRAS^{mut}$ syngeneic model. Genetic and pharmacological manipulations indicated that $HRAS^{mut}$ was sufficient to drive invasion in vitro and metastasis in vivo. Targeted proteomic analysis showed that $HRAS^{mut}$ promoted AXL expression via suppressing the Hippo pathway and stabilizing YAP1 activity. Pharmacological blockade of HRAS signaling with the farnesyltransferase inhibitor tipifarnib activated the Hippo pathway and reduced the nuclear export of YAP1, thus suppressing YAP1-mediated AXL expression and metastasis. AXL was required for $HRAS^{mut}$ cells to migrate and invade in vitro and to form regional cLN and lung metastases in vivo. In addition, AXL-depleted $HRAS^{mut}$ tumors displayed reduced lymphatic and vascular angiogenesis in the primary tumor. Tipifarnib treatment also regulate AXL expression and attenuated VEGFA and VEGFC expression, thus regulating tumor-induced vascular formation and metastasis. Our results indicate that YAP1 and AXL are crucial factors for $HRAS^{mut}$-induced metastasis and that tipifarnib treatment can limit the metastasis of HNC tumors with HRAS mutations by enhancing YAP1 cytoplasmic sequestration and downregulating AXL expression.

Keywords

Head and Neck Cancer; HRAS mutation; Metastasis; AXL; Angiogenesis; YAP1; Hippo pathway; Tipifarnib

Introduction

The main causes of mortality from head and neck cancer (HNC) are treatment failure and/or acquired resistance to therapy, which manifests either as local or regional recurrence with cervical lymph node (cLN) metastasis or recurrent disease with distant metastasis (1). Despite advances in chemoradiotherapy and immunotherapy protocols for the systemic treatment of patients with metastatic disease, the five-year survival rate of patients diagnosed with stage III or IV HNC remains low (1–3).

These poor survival rates provide the motivation to examine the molecular alterations associated with cLN and distant metastasis of HNC. Tumor metastasis is a complex and multi-step process (4) that includes numerous cellular processes, such as apoptosis, invasion,

and migration, which must be activated/employed by tumor cells to establish metastatic disease (4,5). Gene expression profiling of primary and metastatic HNC has identified several genes that are associated with metastatic processes, including the epithelial-mesenchymal transition, stemness, microvascular angiogenesis and lymphogenesis, extracellular matrix degradation, resistance to cell death, and metabolic reprograming, and thus contribute to regional and distant metastasis in HNC patients (6,7). The HRAS mutation ($HRAS^{mut}$) is an important oncogenic driver found in 7% of human papilloma virus-negative HNC patients (8) and in 15% of patients with recurrent metastatic disease (9). The major hot spot mutations in HRAS occur at codons 12, 13 and 61, being frequently detected in cancers of the salivary glands at Q61 and of the oral cavity at G12 (8). The frequency of mutations in HRAS increases after the acquisition of resistance to treatment with cetuximab, an epidermal growth factor receptor inhibitor (10). While in cancer types other than HNC, where HRAS is known to be central protein in metastases signaling cascades (11,12), the molecular mechanisms by which $HRAS^{mut}$ induces cLN and distant metastasis in HNC remains elusive.

In light of the high frequency of HRAS mutations in HNC patients with advanced-stage disease, we sought to elucidate the intracellular machinery enhancing cLN and lung metastasis in these patients. Thus, to comprehensively study the mechanism of $HRAS^{mut}$ on HNC progression and metastasis, we performed genetic and pharmacological manipulations to block HRAS function and its downstream signaling effectors in $HRAS^{mut}$ cell lines, patient-derived xenografts (PDXs), and a novel syngeneic $HRAS^{mut}$ models.

Materials and Methods

Human cell lines

The HRAS-mutant human HNC cell lines, HN31 (G12D), UMSCC17B (Q61L), and CAL33 (Leibniz Institute DSMZ-German Collection of Microorganisms and Cell Cultures, GmbH, Germany), were maintained at 37 °C in a humidified atmosphere of 5% CO_2 in the relevant medium supplemented with 1% L-glutamine 200 mM, 100 units each of penicillin and streptomycin, and 10% fetal bovine serum (FBS). No mycoplasmas were detected with the Mycoplasma Detection Kit (PCR) (HyLabs, Rehovot, Israel).

Primary culture of mice tongue cells

Fresh tongue tissues from male KRT14 Cre mice were washed with Hanks' balanced salt solution (HBSS) or phosphate-buffered saline (PBS), cut into small pieces with sterile scissors, and treated with an enzyme mixture of collagenase (10 mg/mL; Thermo Fisher Scientific, catalog 17104019), hyaluronidase (1 mg/mL; MilliporeSigma, catalog H3506), and DNase (200 U/mL; Thermo Fisher Scientific, catalog18047019). The tissues were dissociated using the gentleMACS™ dissociator. Cells were filtered through a 70-μm cell strainer, centrifuged (300 g, 5 min), and cultured in DMEM high glucose medium. The cultures were stained for the epithelial markers, cytokeratin 14 and E-cadherin, for verification of epithelial origin. All antibodies used in this study has been listed in Supplementary Table 1.

Transduction of primary cells

The concentrated pTomo $HRAS^{V12}$ shp53 (13) (Supplementary Fig. 1A) lentivirus was used to transduce primary tongue cells in the presence of 8 μg/mL of Polybrene (Santa Cruz). After 48 h of transduction, the medium was replaced with fresh medium without virus. Non-transduced cells eventually die after 10 days, and only transduced cells survive after 14 days. Only cells that were GFP^+/RFP^- (green fluorescent $protein^+$/red fluorescent $protein^-$) were considered to be transduced, because only epithelial cells with $KRT14^+$ express Cre, and Cre helps to cleave RFP. Primary tongue cells transduced with this oncogenic vector expressed only GFP because the expression of HRAS is regulated by Cre.

Production of murine sgAXL CRISPR knockout cell lines

Lentiviruses were created by transfecting HEK293 cells with the viral plasmids psPAX2, pMD2.G, and lenticrispr V2 with sgRNAs, i.e., a control sequence (shCT) or either of the 3 different sequences for the silencing of AXL expression (sgAXL1, sgAXL2 and sgAXL3, in-house constructed plasmids) using PEI as described in the Supplementary Materials and Methods. Viruses were collected after 48–72 h and used for cell infection. Cells were seeded in 6-well plates (150,000 cells per well) and infected with the lentiviruses in the presence of Polybrene (MilliporeSigma, 5G-H9268). Cells were selected with puromycin (Thermo Fisher Scientific, A11138-03).

Protein array analysis

Cell lysates were analyzed for 84 oncogenes using the Proteome Profiler Human Oncogene Protein Array kit (R&D systems, Minneapolis, MN, USA) according to the manufacturer's instructions. In brief, cell lysates were prepared using lysis buffer from the relevant array kit, and protein concentration was measured by Bio-Rad protein assay. Cell lysates diluted in the array buffer were incubated with the ready-to-use pre-coated array membranes (blocked in blocking buffer provided with the kit) overnight at 4 °C on a rocking platform shaker. The array membranes were washed three times (10 min) with washing buffer (provided with the kit) to remove any unbound proteins. The membranes were then incubated with the detection antibody cocktail for 1.5 h at room temperature with shaking. The membranes were washed again (3 × 5 min each) with washing buffer and further incubated with diluted streptavidin-HRP for 30 min at room temperature with shaking. The excess buffer was removed, and the protein spots were detected by chemiluminescence 1 min after exposure to the Chemi Reagent mix (from the kit). The arrays were visualized, and images were captured by Azure C300 Chemiluminescent Western Blot Imaging System (Azure Biosystems). The densitometric analysis of the protein array was performed using Image J software with the Protein Array Analyzer plugin (14).

Animal studies

C57/BL6 mice were purchased from Envigo. NOD.Cg-Prkdc Il2rg/SzJ (NSG^{TM}) and KRT14 Cre mice were purchased from The Jackson Laboratory. Mice were housed in air-filtered laminar flow cabinets with a 12 h/12 h light/dark cycle and were fed food and water ad libitum. Mice were maintained and treated according to the institutional guidelines of Ben-Gurion University of the Negev. Animal experiments were approved by the

Institutional Animal Care and Use Committee (IACUC) (IL.80-12-2015 (E), IL.29-05-2018 (E), IL.43-06-2019 (E), IL.44-06-2019 (E)).

PDX development and maintenance

$HRAS^{mut}$ HNC PDX samples, namely, PDX1 (HN11-6062) and PDX2 (HN13-7313) harboring G12S and G13R mutations in HRAS, respectively, were first transplanted subcutaneously (s.c.) into the flanks of 6-week-old NSG mice. Upon successful tumor engraftment, tumors were expanded and retransplanted into other NSG mice. About 3 weeks after the second transplantation, each tumor was excised and a single-cell suspension was prepared. For the experiments, 3×10^6 cells were injected into the lips of NSG mice.

Spontaneous metastasis model

Orthotropic models were established by injecting 1×10^6 $HRAS^{mut}$ human or murine tumor cells or their AXL modulated cells into the lips of C57/BL6 or NSG mice. Tumors were measured with a digital caliper twice a week, and tumor volumes were determined according to the formula: length × $width^2$ × (π/6). At the end of the experiment, when the tumors had reached 500 mm^3 in size, the animals were sacrificed by exposing them to CO_2 inhalation. The tumors, draining cLNs, and lungs were harvested for investigation.

Drug efficacy studies

Animals were randomized into 2 or 4 groups of 5–6 mice per group, depending on the particular *in vivo* metastasis or drug efficacy experiment. When the tumors reached 100 mm^3 in size, the animals were treated orally with tipifarnib (60 mg/kg/twice daily), or R428 (50 mg/kg/twice daily) (provided by BerGenBio) in a vehicle of 0.5% carboxymethylcellulose (Millipore Sigma, Burlington, MA, USA), as indicated in the Results section. Tumors were measured with a digital caliper twice a week, and tumor volumes were determined as described above. At the end of the experiment, animals were sacrificed by exposing them to CO_2 inhalation, and the tumors, cLNs, and lungs were harvested for investigation. Measurements of tumor volumes are given either as average tumor volume ± SEM or as values normalized to initial volumes and presented as an averaged percentage of the initial volumes ± SEM. Harvested tissues were fixed in 4% paraformaldehyde (PFA) overnight and stored in 70% ethanol for further investigation. Serial sections of the lungs were stained with H&E for examining metastasis.

HUVEC maintenance

HUVECs were obtained from ScienCell Research Laboratories (San Diego, CA, USA) (No. 8000) and were grown in endothelial culture medium (No. 1001, ScienCell) containing 5 % FBS (No. 0025), 1 % endothelial cell growth supplement (No. 1052) and 1 % penicillin/streptomycin solution (No. 0503) in 5 % CO_2 at 37 °C. Cells were used in experiments between passages 2 and 5.

Conditioned media.

$HRAS^{mut}$ AXL knock down/knockout cells were allowed to grow to a confluence of 80%. After they reached confluence, the medium was replaced with a serum-free DMEM. The

conditioned medium was collected after 48 h of incubation and centrifuged at 2,000 rpm for 15 min to remove cell debris. The supernatant, i.e., the conditioned medium, was stored at −80 °C until use.

For tipifarnib and R428 conditioned media. $HRAS^{mut}$ human cell line HN31 and murine cells were allowed to grow to a confluence of 80%. After they reached confluence, the cells were treated with DMSO or tipifarnib (100nM/1μM) / R428 (2μM) for 24h. After 24h post treatment, the cells were washed with PBS thrice and supplemented with serum-free DMEM. The conditioned medium was collected after 48 h of incubation and centrifuged at 2,000 rpm for 15 min to remove cell debris. The supernatant, i.e., the conditioned medium, was stored at −80 °C until use.

Statistical analysis

Statistical analysis was performed using GraphPad Prism software (version 9), and values are presented as means ± SEM. For comparisons between two groups, P values were calculated by an unpaired t-test. One-way ANOVA was calculated using Tukey's multiple comparison test for experiments with more than two groups. P values of 0.05 (*), 0.01 (**), 0.001 (***), and 0.0001 (****) were considered statistically significant.

Data Availability Statement

The data generated in this study are available within the article and its supplementary data files. Additional data is available on request from corresponding author. Detailed materials and methods are provided as Supplementary Materials and Methods

Results

Mutated HRAS enhances HNC cell metastasis via switching off the Hippo pathway and activating the YAP1-AXL axis

To explore whether HRAS mutations potentiate invasiveness of HNC cell line *in vitro*, we performed a gain-of-function study in which $HRAS^{mut}$ was genetically incorporated (by using overexpression of the pTomo $HRAS^{V12}$ vector (13)) into wild-type (WT) non-metastatic HRAS Cre-expressing CAL33 (CAL33 Cre^{+}) cells, followed by determination of tumor cells migration and invasion capability (Fig. 1A; Supplementary Fig. 1A and 1B). These *in vitro* studies showed that CAL33 Cre^{+} $HRAS^{V12+}$ cells exhibited enhanced migration and invasive potential compared to CAL33 Cre^{+} cells (Fig. 1B). In reciprocal studies, we examined whether silencing HRAS in $HRAS^{mut}$ cells inhibits their invasive capability. We knocked down HRAS in the metastatic G12D-$HRAS^{mut}$ HNC HN31 cell line by using RNA interference (RNAi) (Fig. 1C; Supplementary Fig. 1C); in those experiments, a reduction in the invasion and migration capability of the knocked-down tumor cells was observed compared to cells transfected with scrambled/control RNAi (Fig. 1D). Notably, knockdown of HRAS did not affect the proliferation of HN31 tumor cells (Supplementary Fig. 1D).

To identify the mechanism by which $HRAS^{mut}$ induces enhanced migration/invasion *in vitro*, we used the human oncogene protein array for comparing i) proteins expressed

by non-metastatic CAL33 Cre^+ cells vs. metastatic CAL33 Cre^+ $HRAS^{V12+}$ cells and ii) proteins expressed by HN31 metastatic $HRAS^{mut}$ cells silenced with HRAS-RNAi vs. cells treated with scrambled-RNAi (Fig. 1E). By keeping a cut-off value of the fold change of more than 1 with a significance of $P<0.001$, we identified 17 altered proteins in CAL33 Cre^+ $HRAS^{V12+}$ and three proteins in HN31 cells that were altered under HRAS-silencing conditions. Among the proteins that were altered in response to HRAS modulation, the most common were AXL and PECAM-1: their expression increased in CAL33 Cre^+ $HRAS^{V12+}$ vs. CAL33 Cre^+ and declined in HRAS-RNAi HN31 cells vs. HRAS-scrambled RNAi cells (Fig. 1F). AXL is a well-studied receptor tyrosine kinase (RTK) involved in the epithelial-to-mesenchymal transition (EMT) and in metastasis (15), but the role of $HRAS^{mut}$ in regulating AXL expression and in enhancing migration/invasion and metastasis has not been previously described. YAP1 is a known transcriptional activator of AXL expression (16) and remarkably an examination of The Cancer Genome Atlas (TCGA) HNC cohorts revealed a strong correlation between AXL and YAP1 expression (Supplementary Fig. 1E). Thus, we hypothesized that $HRAS^{mut}$ regulates the AXL expression through YAP1. To test this hypothesis, we investigated AXL and YAP1 expression in CAL33 and HN31 cells with overexpression or knockdown of mutated HRAS. We found a concomitant modulation in the expression levels of YAP1 and AXL in these tumor cells with dysregulation of $HRAS^{mut}$ (Fig. 1G and H; Supplementary Fig. 1F and 1G). We then explored whether YAP1 regulates AXL expression and whether this determines the migration and invasion potential of $HRAS^{mut}$ HN31 cells. Silencing of YAP1 resulted in downregulation of AXL expression (Fig. 1I; Supplementary Fig. 1H) and a reduction in the ability of the cells to migrate and invade (Fig. 1J). As $HRAS^{mut}$ can regulate the Hippo pathway and YAP1 expression and activity (17), we analyzed the activation status of the Hippo pathway in $HRAS^{mut}$-HN31 cells treated with siHRAS and siControl. We found that silencing HRAS expression activated the Hippo pathway, as indicated by an increase of pLATS1 and pMST1/2, the major activators of Hippo pathway. Moreover, the reduction of YAP1 expression was associated with increased phosphorylation of YAP1 at serine 109, 127 and 397, which impacted the cytoplasmic retention of YAP1 and its subsequent degradation (18) (Fig. 1K; Supplementary Fig. 1I).

We then explored whether pharmacological inhibition of HRAS signaling could induce the same phenotype as that obtained by knocking down HRAS. Blocking HRAS signaling in $HRAS^{mut}$-HN31 cells with tipifarnib, a farnesyl transferase inhibitor, reduced AXL and YAP1 expression (Fig. 1L; Supplementary Fig. 1J) and lowered the invasive potential of these cells (Fig. 1M). Finally, we showed that tipifarnib treatment activated the Hippo pathway and increased the phosphorylation of YAP1 at positions serine 109, 127 and 397 (Fig. 1N; Supplementary Fig. 1K) and also reduced the nuclear expression of YAP1 (Fig. 1O; Supplementary Fig. 1L). These findings indicate that $HRAS^{mut}$ regulates AXL expression by switching off the Hippo pathway, increasing nuclear export and hence activity of YAP1, thus increasing the invasive potential of cancer cells.

Metastasis potential of $HRAS^{mut}$ cells is associated with AXL and YAP1 overexpression

To test the spontaneous metastasis of $HRAS^{mut}$ tumors, we injected CAL33 Cre^+ or CAL33 Cre^+ $HRAS^{V12+}$ cells into the lips of immunodeficient NSG mice, measured primary

tumor growth over time (Fig. 2A), and quantified the cLN and lung metastasis when the tumors reached ~500 mm^3 in size. CAL33 Cre^+ $HRAS^{V12+}$ cells exhibited enhanced metastatic potential, as shown by the enlarged cLNs and the greater number of lung micro-metastasis foci in CAL33 Cre^+ $HRAS^{V12+}$-injected NSG mice vs. CAL33 Cre^+-injected mice (Fig. 2B). Immunohistochemistry staining for tumor cells confirmed the accumulation of tumor cells in the cLNs and lungs of the mice (Fig. 2C, and Supplementary Fig. 2A). To show that our findings were reproducible in independent $HRAS^{mut}$ HNC models, we performed spontaneous metastasis studies using cell-line-derived xenografts (CDXs) and PDXs possessing HRAS mutations. To develop CDXs, we injected $HRAS^{mut}$ UMSCC17B (Q61L) or HN31 cells orthotopically into the lips of NSG mice. The UMSCC17B cells grew more rapidly (Fig. 2D), but the mice exhibited a low number of enlarged cLNs, and only 4 of the 12 mice showed micro-metastases. In contrast, growth of the HN31 cells was slower, but these cells exhibited enhanced metastatic capacity, reaching the cLNs and the lungs more efficiently with macro-metastases (Fig. 2E, and Supplementary Fig. 2B). Western blot analysis of the cell lines showed that the metastatic HN31 cells expressed higher levels of YAP1 and AXL than the weakly metastatic UMSCC17B cells (Fig. 2F; Supplementary Fig. 2C). To study the metastasis of $HRAS^{mut}$ PDXs, we used PDX1 and PDX2, the two PDXs described in Materials and Methods. Briefly, we injected 3×10^6 single-cell suspensions of PDXs into the lips of NSG mice and allowed tumors to form. When the tumors reached ~500 mm^3 in size, the mice were sacrificed, and the number of enlarged cLNs and the number of metastatic foci in the lungs of each tumor-bearing mouse were counted. PDX1 (HN11-6062) showed low metastatic potential with no cLN metastases, but lung micro-metastases were evident in 2 of 12 mice. In contrast, the metastatic potential of PDX2 (HN13-7313) was significantly higher, as all 12 mice exhibited cLN metastases, and 5 of the 12 mice developed lung metastases (Fig. 2G and 2H, and Supplementary Fig. 2D). Western blot analysis of the PDXs showed that the metastatic PDX2 expressed higher levels of AXL and YAP1 than the less-metastatic PDX1 (Fig. 2I; Supplementary Fig. 2E). These findings provide support for the association of AXL and YAP1 expression with the enhanced metastasis potential of $HRAS^{mut}$ HNC models.

Because treatment of $HRAS^{mut}$ cells with tipifarnib reduced YAP and AXL expression and reduced cell migration and invasion *in vitro*, we posited that tipifarnib treatment of mice bearing metastatic $HRAS^{mut}$-HN31 tumors would also attenuate spontaneous metastasis into the cLNs and lungs of the mice. Indeed, we found that daily treatment of HN31 tumor-bearing mice with tipifarnib resulted in growth retardation of the primary tumor (Fig. 2J) accompanied by a reduction of enlarged cLNs and lung macro-metastasis (Fig. 2K and 2L).

AXL expression potentiates metastasis of $HRAS^{mut}$ HNC cells

We next set out to determine whether AXL expression is required for metastasis of $HRAS^{mut}$ HNC. To this end, we initially knocked down AXL expression in the metastatic HN31 cell line (Fig. 3A; Supplementary Fig. 3A) and then tested the ability of the tumor cells to migrate/invade *in vitro* and metastasize *in vivo*. The *in vitro* experiment showed that $HRAS^{mut}$-HN31 cells with AXL knockdown (shAXL) were less invasive than HN31 control cells (shCT) (Fig. 3B, and Supplementary Fig. 3B). We further showed that AXL

activation by its ligand Gas6 is required for the migration of HN31 tumor cells and that the upregulation of Gas6 in shAXL-HN31 tumor cells was not sufficient to facilitate cell migration (Fig. 3C and Supplementary Fig. 3C). *In vivo* experiments revealed that AXL knockdown enhanced the primary growth of $HRAS^{mut}$-HN31 xenografts (Fig. 3D), but these cells lost the ability to promote metastasis to the cLNs and lungs (Fig. 3E, and Supplementary Fig. 3D). Transwell migration assay showed that pharmacological inhibition of AXL with R428, a known potent and selective inhibitor of AXL, reduced the ability of the HN31 cells to migrate and invade (Fig. 3F). This reduction in invasion and migration was associated with a plasticity change of the mesenchymal-like phenotype of HN31 from N-cadherin high and E-cadherin low cells to an epithelial-like phenotype with high E-cadherin and lower N-cadherin, but with no inhibition of the MAPK or the PI3K/AKT pathway (Supplementary Fig. 3E). Finally, in HN31-tumor-bearing mice that were treated twice daily with R428, growth of the primary tumor was not delayed and there was no significant impact on tumor volumes (Fig. 3G), but there was a reduction in cLN and lung metastasis (Fig. 3H). Similar results were also obtained in PDX2-tumor-bearing mice treated with R428 (Fig. 3I and 3J). These results suggest that targeting AXL signaling impedes the metastasis capability of $HRAS^{mut}$ HNC tumor cells.

To explore whether AXL has the ability to enhance metastasis in $HRAS^{mut}$ HNC cell lines, we overexpressed (OE) AXL in the weakly metastatic UMSCC17B cells (Supplementary Fig. 3F) and determined their invasive potential *in vitro* and in mice. The *in vitro* experiment showed that overexpression of AXL enhanced the migration and invasion of UMSCC17B cells (Fig. 3K). The *in vivo* experiment in NSG mice showed similar growth kinetics for UMSCC17B-OE-AXL cells and UMSCC17B cells (Fig. 3L), but UMSCC17B-OE-AXL-tumor-bearing mice exhibited an increased number of enlarged cLNs. Five of six mice bearing UMSCC17B-OE-AXL tumors showed lung metastasis with multiple foci compared to AXL-null vector-UMSCC17B tumors (Fig. 3M, and Supplementary Fig. 3G). Thus, overexpression of AXL potentiates the metastasis capability of $HRAS^{mut}$ HNC tumor cells.

Depleting AXL in $HRAS^{mut}$ tumors reduces blood vessel formation and lymphangiogenesis by downregulation of the expression of vascular endothelial growth factors (VEGF) A and C

To get further mechanistic insight on metastasis cascade, we hypothesized that $HRAS^{mut}$ HNC cells that spread from the primary lesion to the cLNs and distant organs must first invade the vascular system and survive anoxic conditions. Analysis of the TCGA database support this hypothesis as HNC patients with mutated or amplified HRAS express high levels of lymphangiogenesis and angiogenesis signatures (Supplementary Fig. 4A). Moreover, comparing gene expression of metastatic HNC (POG570) (19) and non-metastatic HNC (TCGA) also show HRAS overexpression, lymphangiogenesis and angiogenesis activation in metastatic disease (Supplementary Fig. 4B). To test this hypothesis in our cancer models, we determined whether $HRAS^{mut}$ tumors with AXL overexpression are enriched with lymphatic and blood vessels compared to tumors with low expression of AXL. Indeed, staining shCT and shAXL HN31 tumors with LYVE-1 (marker for lymphangiogenesis) and CD31 (marker for angiogenesis) revealed a lower number of stained cells in shAXL tumors (Fig. 4A). To explore the mechanism underlying

such differences, we searched the TCGA data set for VEGFA or VEGFC, both important angiogenesis factors involved in vessel formation in HNC patients (20–22), which may display a correlation between mRNA levels of AXL. The results revealed that AXL expression is strongly associated with VEGFC (Supplementary Fig. 4C), and we therefore posited that AXL-intact cells express and secrete VEGFs that support the angiogenesis process. The conditioned medium derived from AXL-intact shCT HN31 cells enhanced tube formation of HUVECs *in vitro*, but the conditioned medium derived from shAXL tumor cells showed reduced ability to induce tube formation of HUVEC (Fig. 4B). The base-line mRNA expression of VEGFA and VEGFC in high- and low-AXL-expressing tumor cells (shCT and shAXL) showed that cells with down-regulation of AXL express lower mRNA levels of VEGFC and VEGFA compared to AXL-intact cells (Fig. 4C). Reduction of VEGFA and VEGFC was also observed in HN31 tumor cells treated with R428, and the conditioned medium (CM) of R428-treated cells induced less tube formation than the CM obtained from DMSO-treated cells (Fig. 4D and 4E). Moreover, neutralization of VEGFA using Avastin in the CM of shCT cells was sufficient to reduce tube formation (Fig. 4F), and supplementation of recombinant VEGFA in the CM of shAXL cells enhanced the formation of tubes by HUVEC (Fig. 4G).

Since tipifarnib treatment is known to reduce tumor angiogenesis in $HRAS^{mut}$ tumors (23), we explored whether tipifarnib treatment reduces VEGFA and VEGFC expression in both human and murine HRAS mutant lines. qPCR analysis showed that treatment of $HRAS^{mut}$ cells with tipifarnib reduced VEGFA and VEGFC mRNA expression in both cell lines (Fig. 4H). Lastly, in a tube-formation assay, we exposed HUVECs to conditioned media collected from tumor cells subjected to 24 h of pre-treatment with tipifarnib (or DMSO as control). The conditioned medium of the HN31 cells pre-treated with tipifarnib supported low tube formation compared to the conditioned medium of DMSO-pretreated $HRAS^{mut}$ cells (Fig. 4I). These results suggest that AXL expression in $HRAS^{mut}$ tumor cells augments the neovascularization process thus facilitating to the process of metastasis.

AXL is essential for metastasis in a syngeneic $HRAS^{mut}$ HNC model

Metastasis is a multi-stage process, affected by multiple cell types in the microenvironment. To validate our findings in a physiologically relevant system we generated an HRAS mutant cell line by lentiviral infection of primary tongue cells isolated from KRT14 Cre mice, and established a novel immune competent murine model of HNC (Fig. 5A, and Supplementary Fig. 5A). The novel murine HNC cell line was designated $HRAS^{V12}$ shp53 EpT ($HRAS^{V12}$ shp53 epithelial tongue) (Supplementary Fig. 5B and C). We confirmed the expression of HRAS and p53 knockdown by western blotting and showed that the infection of normal tongue cells with the lentivirus induced an EMT phenotype with high expression of N-cadherin, AXL and YAP1 (Fig. 5A; Supplementary Fig. 5D). The transformed $HRAS^{V12}$ shp53 EpT cells showed a tumorigenic phenotype compared to normal tongue cells, as was evident from the uncontrolled cell proliferation and the ability to form colonies and grow in anchorage-independent 3D cultures (Supplementary Fig. 5F–G). Similarly, compared to normal epithelial cells, $HRAS^{V12}$ shp53 EpT cells exhibited enhanced metastatic activity, with the ability to migrate and invade, as shown in transwell assays (Supplementary Fig. 5H). The transform $HRAS^{V12}$ shp53 EpT cells displayed an

inactivation of Hippo pathway, as indicated by the decrease of pLATS1 and pMST1/2, the major activators of Hippo pathway. Moreover, the increase of YAP1 expression was associated with decreased phosphorylation of YAP1 at serine 109, and 397 (Supplementary Fig. 5I). *In vivo* injection of $HRAS^{V12}$ shp53 EpT cells into the lips of wild-type (WT) C57/B6 mice resulted in measurable tumor growth after seven days (Supplementary Fig. 5J). Histological examination revealed poorly differentiated tumors with a spindle morphology and mesenchymal-type phenotype attributes, indicating an aggressive type of HNC (Supplementary Fig. 5K). To further study the spontaneous metastasis potential of $HRAS^{V12}$ shp53 EpT cells, we injected cells into the lips of NSG or WT mice. Interestingly, although the tumors exhibited the same growth kinetics in WT and NSG mice (Fig. 5B), the metastatic burden in the lungs was higher in the NSG mice than that in the WT mice (Fig. 5C). In contrast, the metastatic burden in the cLNs was enhanced in WT mice (Fig. 5C). cLN metastasis in WT mice was verified by flow cytometry and histology (Supplementary Fig. 5L and 5M). Importantly, all NSG mice injected with $HRAS^{V12}$ shp53 EpT cells exhibited lung macro-metastases, while in the WT mice, mainly micro-metastases were detected in half of the mice, as confirmed by staining with GFP (Supplementary Fig. 5M). These results indicate that $HRAS^{V12}$ shp53 EpT cells induce a local immune suppressive environment that facilitates rapid tumor growth, but upon tumor cell dissemination from the primary lesion the anti-tumor immunity machinery potentially eradicated such circulating tumor cells.

We then went on to explore the role of AXL in the syngeneic $HRAS^{V12}$ shp53 EpT model by generating three AXL-knockout clones with CRISPR-Cas9. The knockout of AXL was confirmed by flow cytometry and western blotting (Supplementary Fig. 5N and 5O). Subsequent studies with two of these clones, sgAXL1 and sgAXL2 showed that knockout of AXL in $HRAS^{V12}$ shp53 EpT cells resulted in a reduction of invasion and migration potential *in vitro* (Supplementary Fig. 5N) and in lung micro-metastasis in WT mice and macro-metastasis in NSG mice (Fig. 5D and 5E).

We then explored whether the $HRAS^{V12}$ shp53 EpT AXL knockout tumors display reduced angiogenesis, as observed in human $HRAS^{mut}$ AXL knockdown HNC. Staining sgCT and sgAXL $HRAS^{V12}$ shp53 EpT tumors with LYVE-1 and CD31 revealed a lower number of stained cells in sgAXL tumors (Fig. 5F). Similar to the results obtained for the human $HRAS^{mut}$ line, the conditioned medium derived from sgAXL tumor cells showed reduced ability to induce tube formation of HUVECs (Fig. 5G) and vessel formation *in vivo* (Supplementary Fig. 5P). qPCR analysis of the AXL knockout $HRAS^{V12}$ shp53 EpT cells also confirmed that downregulation of AXL leads to reduced VEGFA and VEGFC expression (Fig. 5H). These findings reiterate the potential role of AXL in $HRAS^{mut}$ HNC cells in governing metastasis.

Pharmacological inhibition of AXL/HRAS signaling attenuates metastasis in a syngeneic model

We next explored the effect of AXL and HRAS inhibition on metastasis in $HRAS^{V12}$ shp53 EpT cells. Pharmacological inhibition of AXL activity by R428 blocked the metastatic capability of $HRAS^{V12}$ shp53 EpT cells *in vitro* (Fig. 6A). *In vivo*, treatment of tumor-

bearing mice with R428 did not induce tumor growth arrest but reduced metastasis burden in both WT and NSG mice (Fig. 6B and 6C, and Supplementary Fig. 6A). These results provide further support for our premise that AXL signaling is required for metastasis but not for primary tumor growth.

To test the effect of tipifarnib on $HRAS^{V12}$ shp53 EpT cells, we initially explored the sensitivity of the cells to this agent and showed that the half-maximal inhibition concentration is 1.1 μM (Supplementary Fig. 6B). We next step investigated whether HRAS signaling in $HRAS^{V12}$ shp53 EpT cells determines AXL and YAP1 expression and metastasis potential. Western blot analysis showed that treatment of the tumor cells with tipifarnib reduced both AXL and YAP1 expression (Supplementary Fig. 6C and 6D). To explore the effect of tipifarnib on invasion and migration *in vitro*, we treated the $HRAS^{V12}$ shp53 EpT cells with 1 μM tipifarnib and quantified the number of cells that migrated/invaded through the transwell membrane. The transwell migration/invasion assay showed that tipifarnib treatment reduced the ability of the $HRAS^{V12}$ shp53 EpT cells to migrate and invade (Fig. 6D). Lastly, we tested the efficacy of tipifarnib *in vivo* in WT and NSG mice. Tipifarnib treatment of mice bearing $HRAS^{V12}$ shp53 EpT tumors inhibited tumor growth, and markedly reduced cLN and lung metastasis in both WT and NSG mice in both models (Fig. 6E and 6F).

Taken together, our findings support a novel molecular mechanism of metastasis in HNC harboring HRAS mutation (Fig. 7). Specifically, $HRAS^{mut}$ stabilizes YAP1 activity to increase AXL expression by turning off the Hippo pathway. The enhanced AXL expression, in turn, accelerates the metastasis process of HNC by enhancing cell migration, invasion, and vascular/lymphatic angiogenesis. Targeting AXL with R428 in HNC, did not reduce cell proliferation, but weakened vascular/lymphatic angiogenesis, and reversed EMT process, resulting in reduced metastasis. Targeting HRAS with tipifarnib activates the Hippo pathway, enhances YAP1 cytoplasmic retention, and reduces YAP1 nuclear export and AXL expression, thereby reducing HNC metastasis.

Discussion

HNC is characterized by a poor prognosis with a high risk of local recurrence and distant metastasis (1,24,25). Here, we showed that mutations in HRAS promoted cancer aggressiveness and metastasis, findings that are in line with the oncogenic effect of RAS family members and their signaling pathways in other cancer types (26–31). Our study provided novel insights into the role(s) of $HRAS^{mut}$ in promoting metastasis and identify the underlying signaling mechanism. Specifically, we found that $HRAS^{mut}$ acts through a Hippo-YAP1-AXL axis, which regulates cLN and distant metastasis in HNC.

Metastasis is a complex process that starts when cancer cells acquire the ability to invade adjacent organs and/or migrate through the bloodstream or lymphatic system to distant sites, where they survive and colonize (32). The current study shows that ectopic expression of the HRAS mutation in HNC cells markedly increased their invasive ability both *in vitro* and *in vivo* (Figs. 1 and 2), in keeping with previous reports showing the role of HRAS in promoting the EMT (33,34) and cell invasion in urothelial and gastric cancer (35,36).

A key finding in the current study was the upregulation of AXL expression in HRAS^{mut} HNC cells. AXL is a member of the TAM family of receptors (Tyro, AXL, MER) and is also a mesenchymal marker implicated in cancer cell proliferation, migration, angiogenesis, metastasis, and therapeutic resistance of HNC (37–40). AXL is also expressed in the partial epithelial-mesenchymal transition (pEMT), a prerequisite plasticity stage for metastasis that promotes local invasion in HNC (41). Genomic and transcriptomic analyses of the TCGA cohort showed that HNC tumors harboring the HRAS mutation were clustered as mesenchymal/basal subtypes (42), with AXL expression being higher in those clusters. In a previous study in basal-like breast cancer cells, it was shown that HRAS-induced EMT was dependent on the upregulation of vimentin, which mediated invasion and migration, in part, through upregulating AXL (43). In the current study, we showed a different mechanism of regulation of AXL expression by HRAS^{mut}, which involves activation of YAP1 and the inhibition of the Hippo pathway. Using HRAS^{mut} HNC cell lines, we demonstrated that AXL expression is regulated by YAP1, and we thus extensively studied the role of AXL expression in determining metastasis to the cLNs and lungs in mice. Notably, the levels of phosphorylated AXL were undetectable, so it was not possible to examine the role of AXL activation in the metastasis of HRAS^{mut} HNC. The overexpression of AXL in AXL-null HRAS^{mut} HNC cells with a low metastatic colonization potential led to augmented migratory and invasive abilities *in vivo*. The AXL-depleted models showed reduced metastasis, corroborating studies from other AXL-depleted cancer lines (44–46). In the current study, we also demonstrated that AXL depletion blocked neovascularization, thus preventing the movement of tumor cells to draining lymph nodes and the bloodstream. Pharmacological inhibition of AXL reduced the metastatic burden but did not curtail tumor progression. These results indicate that AXL expression in HRAS^{mut} HNC is probably a prerequisite for the metastasis process, but these tumor cells are resistant to anti-AXL therapies, as has been shown for resistance to erlotinib (37). Our *in vivo* data suggests that inhibition of AXL signaling alone is insufficient to eliminate tumors in HRAS-mutant HNC cancers, and more potent treatment strategies are required.

Since AXL is one of the downstream targets of YAP/TAZ (16,47), the known crosstalk between AXL and YAP1 in promoting tumor progression in HNC (48) motivated us to examine the HRAS-YAP1-AXL axis. RAS can regulate YAP1 activity by multiple mechanisms, namely through: (i) its effector, PI3K (49), (ii) up-regulation of RTKs or RTK ligands (50), (iii) SUMOylation of ubiquitin thioesterase (OTUB2) (51), (iv) down-regulation of MST1/2 activity by inducing the formation of inactive MST1/MST2 heterodimers (17), and/or (v) downregulation of suppressor of cytokine signaling 6 (SOCS6) (52). YAP1 is a potent transcriptional co-activator that lacks direct DNA-binding activity but modulates gene expression by binding to other transcription factors. As documented previously, phosphorylation of YAP1 at various serine residues have various biological implications on YAP1 activity. For example, phosphorylation of serine at 109 and 127 leads to YAP1 cytoplasmic retention (18,53) whereas at 381/397 it causes ubiquitination degradation of YAP1, which is dependent on the β-transducin repeat-containing E3 ubiquitin protein ligase complex (18,54). Our study shows that HRAS signaling regulates YAP1 activity and stability by turning off the Hippo pathway, and that knocking down HRAS or blocking HRAS signaling with tipifarnib turned on the Hippo pathway, enhanced YAP1

sequestration in the cytoplasm and reduced nuclear localization, which subsequently led to reduction in AXL expression.

HRAS proteins undergo several post-translational modifications that facilitate their attachment to membranes, including the addition of a farnesyl isoprenoid moiety by the enzyme farnesyl transferase (55). Farnesyl transferase inhibitors reduce HRAS membrane localization, leading to decreased GTP-bound HRAS and decreased signaling through RAS effector pathways, thus blocking HRAS signaling (56,57). Among the farnesyl transferase inhibitors, tipifarnib is a potent compound that has demonstrated compelling anti-tumor activity in pre-clinical models (23) and in a heavily pretreated cohort of patients with recurrent/metastatic HNC carrying HRAS mutations (58,59). In this work, we showed for the first time that tipifarnib treatment attenuates the metastatic potential of $HRAS^{mut}$ cells, and we also provided mechanistic insight into the effect of tipifarnib on the Hippo pathway, YAP1 activation, and AXL expression. The efficacy of tipifarnib in preventing primary tumor growth was relatively modest in this study with no regression noted. Previous studies have described mechanisms of resistance to tipifarnib, including activation of the MAPK and PI3K pathways (60). Further investigation is required to explore the efficacy of a treatment combination of tipifarnib and PI3K inhibitors in syngeneic murine-$HRAS^{V12}$ shp53 EpT tumors, as it has been shown that a combination of the two compound's exhibited superior anti-tumor activity in PDXs (61).

The growth of primary tumors and metastatic neoplastic lesions depends strongly on the ability of cancer cells to initiate neovascularization through angiogenesis (62,63). Tumor cells induce angiogenesis by secreting pro-angiogenic factors, such as VEGFs and angiopoietins, and releasing proteolytic enzymes that recruit endothelial cells and cleave extracellular matrices (63). Angiogenesis is thus an integral aspect of the growth, proliferation, and metastasis of HNC and has potential implications for the prognosis and treatment of both localized and recurrent/metastatic HNC (64). For instance, the up-regulation of angiogenic factors, such as VEGFA, VEGFC and VEGFD, typically corresponds to increased vascularity, lymph node metastasis, an inadequate response to cytotoxic chemotherapy, and advanced disease with a poor prognosis in HNC (as reviewed in (65)). It is well documented that oncogenic HRAS functions as a cellular switch that controls angiogenesis and vascular permeability by activating distinct downstream effectors (66,67). Our study is also in line with previous findings in breast cancer (68) that AXL depletion in $HRAS^{mut}$ cells attenuates the expression of the pro-angiogenic factors, VEGFA and VEGFC, thereby reducing vascular and lymphatic angiogenesis. Recent studies on AXL depletion in $HER2^{+}$ breast cancers reveal that, during hypoxia, interfering with AXL reduces HIF-1α levels and AKT phosphorylation, leading to normalizing the blood vessels and thus promotes a proinflammatory microenvironment (45). Our *in vivo* findings on reduced neovascularization and metastasis on AXL depletion also imply the significance of AXL and its involvement in controlling hypoxia-mediated angiogenesis and the tumorigenesis process. Further studies are required to study the role of hypoxia and AXL in $HRAS^{mut}$ HNC.

In summary, our studies revealed that metastasis in $HRAS^{mut}$ HNC is regulated by the stabilization of YAP1 activity and the overexpression of AXL, both of which regulate cell migration, invasion, and vascular/lymphatic angiogenesis. Blocking HRAS signaling

reduces YAP1 activity and AXL expression, which, in turn, downregulate VEGFA and VEGFC expression. Ultimately, we provide evidence that targeting the novel HRAS-YAP1-AXL signaling axis may represent an attractive therapeutic candidate to limit the metastasis of $HRAS^{mut}$ HNC cells.

Supplementary Material

Refer to Web version on PubMed Central for supplementary material.

Acknowledgment

The authors thank Dr Shira Ovadia, Ben Gurion University of the Negev, for her assistance in the animal facility; Mrs Inez and Prof Neta Erez, Tel Aviv University for the critical editing of the manuscript.

Funding

This work was funded by the Israel Science Foundation (ISF, 302/21) (to ME), The United States-Israel Binational Science Foundation (BSF, #2021055 to ME and SJG), ISF and NSFC Israel-China project (to ME and DK #3409/20) and Kura Oncology (to ME). At Memorial Sloan Kettering Cancer Center, support was provided by the NIH/NCI Cancer Center Support Grant P30 CA008748 (to ALH). SJ is the recipient of a PBC post-doctoral fellowship from the Israel Council for Higher Education.

References

1. Pisani P, Airoldi M, Allais A, Valletti PA, Battista M, Benazzo M, et al. Metastatic disease in head & neck oncology. Acta Otorhinolaryngologica Italica 2020;40:S1–86. [PubMed: 32469009]
2. Beckham TH, Leeman JE, Xie P, Li X, Goldman DA, Zhang Z, et al. Long-term survival in patients with metastatic head and neck squamous cell carcinoma treated with metastasis-directed therapy. Br J Cancer 2019;121:897–903. [PubMed: 31649318]
3. Shaikh H, Karivedu V, Wise-Draper TM. Managing Recurrent Metastatic Head and Neck Cancer. Hematol Oncol Clin North Am 2021;35:1009–20. [PubMed: 34226077]
4. Wan L, Pantel K, Kang Y. Tumor metastasis: Moving new biological insights into the clinic. Nat Med 2013;19:1450–64. [PubMed: 24202397]
5. Fares J, Fares MY, Khachfe HH, Salhab HA, Fares Y. Molecular principles of metastasis: a hallmark of cancer revisited. Signal Transduct Target Ther 2020;5:1–17. [PubMed: 32296011]
6. Colella S, Richards KL, Bachinski LL, Baggerly KA, Tsavachidis S, Lang JC, et al. Molecular signatures of metastasis in head and neck cancer. Head Neck 2008;30:1273–83. [PubMed: 18642293]
7. Bhave SL, Teknos TN, Pan Q. Molecular parameters of head and neck cancer metastasis. Crit Rev Eukaryot Gene Expr 2011;21:143–53. [PubMed: 22077153]
8. Novoplansky O, Jagadeeshan S, Regev O, Menashe I, Elkabets M, Segal S. Worldwide Prevalence and Clinical Characteristics of RAS Mutations in Head and Neck Cancer: A Systematic Review and Meta-Analysis. Front Oncol 2022;12:12:838911. [PubMed: 35600380]
9. Reder H, Wagner S, Wuerdemann N, Langer C, Sandmann S, Braeuninger A, et al. Mutation patterns in recurrent and/or metastatic oropharyngeal squamous cell carcinomas in relation to human papillomavirus status. Cancer Med 2021;10:1347–56. [PubMed: 33527763]
10. Braig F, Voigtlaender M, Schieferdecker A, Busch CJ, Laban S, Grob T, et al. Liquid biopsy monitoring uncovers acquired RAS-mediated resistance to cetuximab in a substantial proportion of patients with head and neck squamous cell carcinoma. Oncotarget 2016;7:42988–95. [PubMed: 27119512]
11. Takács T, Kudlik G, Kurilla A, Szeder B, Buday L, Vas V. The effects of mutant Ras proteins on the cell signalome. Cancer Metastasis Rev 2020;39:1051–65. [PubMed: 32648136]

12. Santra T, Herrero A, Rodriguez J, von Kriegsheim A, Iglesias-Martinez LF, Schwarzl T, et al. An Integrated Global Analysis of Compartmentalized HRAS Signaling. Cell Rep 2019;26:3100–3115.e7. [PubMed: 30865897]
13. Friedmann-Morvinski D, Bushong EA, Ke E, Soda Y, Marumoto T, Singer O, et al. Dedifferentiation of neurons and astrocytes by oncogenes can induce gliomas in mice. Science 2012;338:1080–4. [PubMed: 23087000]
14. Carpentier G Dot Blot Analyzer: Software development using the macro language of ImageJ. Proceedings of the ImageJ User and Developer Conference. 2008. page ISBN 2-919941-06-2.
15. Antony J, Huang RYJ. AXL-driven EMT state as a targetable conduit in cancer. Cancer Res 2017;77:3725–32. [PubMed: 28667075]
16. Xu MZ, Chan SW, Liu AM, Wong KF, Fan ST, Chen J, et al. AXL receptor kinase is a mediator of YAP-dependent oncogenic functions in hepatocellular carcinoma. Oncogene 2011;30:1229–40. [PubMed: 21076472]
17. Rawat SJ, Araiza-Olivera D, Arias-Romero LE, Villamar-Cruz O, Prudnikova TY, Roder H, et al. H-ras Inhibits the Hippo Pathway by Promoting Mst1/Mst2 Heterodimerization. Current Biology 2016;26:1556–63. [PubMed: 27238285]
18. Zhao B, Li L, Tumaneng K, Wang CY, Guan KL. A coordinated phosphorylation by Lats and CK1 regulates YAP stability through SCFβ-TRCP. Genes Dev 2010;24:72–85. [PubMed: 20048001]
19. Pleasance E, Titmuss E, Williamson L, Kwan H, Culibrk L, Zhao EY, et al. Pan-cancer analysis of advanced patient tumors reveals interactions between therapy and genomic landscapes. Nat Cancer 2020;1:452–68. [PubMed: 35121966]
20. Boonkitticharoen V, Kulapaditharom B, Leopairut J, Kraiphibul P, Larbcharoensub N, Cheewaruangroj W, et al. Vascular endothelial growth factor a and proliferation marker in prediction of lymph node metastasis in oral and pharyngeal squamous cell carcinoma. Arch Otolaryngol Head Neck Surg 2008;134:1305–11. [PubMed: 19075127]
21. Cohen-Kaplan V, Naroditsky I, Zetser A, Ilan N, Vlodavsky I, Doweck I. Heparanase induces VEGF C and facilitates tumor lymphangiogenesis. Int J Cancer 2008;123:2566–73. [PubMed: 18798279]
22. Sugiura T, Inoue Y, Matsuki R, Ishii K, Takahashi M, Abe M, et al. VEGF-C and VEGF-D expression is correlated with lymphatic vessel density and lymph node metastasis in oral squamous cell carcinoma: Implications for use as a prognostic marker. Int J Oncol 2009;34:673–80. [PubMed: 19212672]
23. Gilardi M, Wang Z, Proietto M, Chilla A, Calleja-Valera JL, Goto Y, et al. Tipifarnib as a precision therapy for HRAS-mutant head and neck squamous cell carcinomas. Mol Cancer Ther 2020;19:1784–96. [PubMed: 32727882]
24. Johnson DE, Burtness B, Leemans CR, Lui VWY, Bauman JE, Grandis JR. Head and neck squamous cell carcinoma. Nat Rev Dis Primers 2020;6:1–22. [PubMed: 31907359]
25. Wise-Draper TM, Bahig H, Tonneau M, Karivedu V, Burtness B. Current Therapy for Metastatic Head and Neck Cancer: Evidence, Opportunities, and Challenges. American Society of Clinical Oncology 2022;42:1–14.
26. Pei L, Melmed S, Scheithauer B, Kovacs K, Prager D. H-ras mutations in human pituitary carcinoma metastases. J Clin Endocrinol Metab 1994;78:842–6. [PubMed: 8157709]
27. Jakob JA, Bassett RL, Ng CS, Curry JL, Joseph RW, Alvarado GC, et al. NRAS mutation status is an independent prognostic factor in metastatic melanoma. Cancer 2012;118:4014–23. [PubMed: 22180178]
28. Boutin AT, Liao WT, Wang M, Hwang SS, Karpinets TV, Cheung H, et al. Oncogenic Kras drives invasion and maintains metastases in colorectal cancer. Genes Dev. 2017;31:370–82. [PubMed: 28289141]
29. Yeh HH, Tseng YF, Hsu YC, Lan SH, Wu SY, Raghavaraju G, et al. Ras induces experimental lung metastasis through up-regulation of RbAp46 to suppress RECK promoter activity. BMC Cancer 2015;15:1–14. [PubMed: 25971837]
30. Wright KL, Adams JR, Liu JC, Loch AJ, Wong RG, Jo CEB, et al. Ras signaling is a key determinant for metastatic dissemination and poor survival of luminal breast cancer patients. Cancer Res 2015;75:4960–72. [PubMed: 26400062]

31. Yaeger R, Cowell E, Chou JF, Gewirtz AN, Borsu L, Vakiani E, et al. RAS mutations affect pattern of metastatic spread and increase propensity for brain metastasis in colorectal cancer. Cancer 2015;121:1195–203. [PubMed: 25491172]
32. Leong SP, Naxerova K, Keller L, Pantel K, Witte M. Molecular mechanisms of cancer metastasis via the lymphatic versus the blood vessels. Clin Exp Metastasis 2022;39:159–79. [PubMed: 34767139]
33. Oft M, Peli J, Rudaz C, Schwarz H, Beug H, Reichmann E. TGF-β1 and Ha-Ras collaborate in modulating the phenotypic plasticity and invasiveness of epithelial tumor cells. Genes Dev 1996;10:2462–77. [PubMed: 8843198]
34. Oft M, Akhurst RJ, Balmain A. Metastasis is driven by sequential elevation of H-ras and Smad2 levels. Nat Cell Biol 2002;4:487–94. [PubMed: 12105419]
35. Wu XY, Liu WT, Wu ZF, Chen C, Liu JY, Wu GN, et al. Identification of HRAS as cancer-promoting gene in gastric carcinoma cell aggressiveness. Am J Cancer Res 2016;6:1935. [PubMed: 27725900]
36. He F, Melamed J, Tang MS, Huang C, Wu XR. Oncogenic HRAS activates epithelial-to-mesenchymal transition and confers stemness to p53-deficient urothelial cells to drive muscle invasion of basal subtype carcinomas. Cancer Res 2015;75:2017–28. [PubMed: 25795707]
37. Giles KM, Kalinowski FC, Candy PA, Epis MR, Zhang PM, Redfern AD, et al. Axl mediates acquired resistance of head and neck cancer cells to the epidermal growth factor receptor inhibitor erlotinib. Mol Cancer Ther 2013;12:2541–58. [PubMed: 24026012]
38. von Mässenhausen A, Brägelmann J, Billig H, Thewes B, Queisser A, Vogel W, et al. Implication of the receptor tyrosine kinase AXL in head and neck cancer progression. Int J Mol Sci 2017;18:7.
39. Brand TM, Iida M, Stein AP, Corrigan KL, Braverman CM, Luthar N, et al. AXL mediates resistance to cetuximab therapy. Cancer Res 2014;74:5152–64. [PubMed: 25136066]
40. Badarni M, Prasad M, Balaban N, Zorea J, Yegodayev KM, Joshua BZ, et al. Repression of AXL expression by AP-1/JNK blockage overcomes resistance to PI3Ka therapy. JCI Insight. 2019; 5(8):e125341. [PubMed: 30860495]
41. Puram SV, Parikh AS, Tirosh I Single cell RNA-seq highlights a role for a partial EMT in head and neck cancer. Mol Cell Oncol 2018;5:01–6.
42. Lawrence MS, Sougnez C, Lichtenstein L, Cibulskis K, Lander E, Gabriel SB, et al. Comprehensive genomic characterization of head and neck squamous cell carcinomas. Nature 2015;517:576–82. [PubMed: 25631445]
43. Vuoriluoto K, Haugen H, Kiviluoto S, Mpindi JP, Nevo J, Gjerdrum C, et al. Vimentin regulates EMT induction by Slug and oncogenic H-Ras and migration by governing Axl expression in breast cancer. Oncogene 2011;30:1436–48. [PubMed: 21057535]
44. Goyette MA, Duhamel S, Aubert L, Pelletier A, Savage P, Thibault MP, et al. The Receptor Tyrosine Kinase AXL Is Required at Multiple Steps of the Metastatic Cascade during HER2-Positive Breast Cancer Progression. Cell Rep 2018;23:1476–90. [PubMed: 29719259]
45. Goyette MA, Elkholi IE, Apcher C, Kuasne H, Rothlin C v., Muller WJ, et al. Targeting Axl favors an antitumorigenic microenvironment that enhances immunotherapy responses by decreasing Hif-1α levels. Proc Natl Acad Sci U S A 2021;118.
46. Du W, Phinney NZ, Huang H, Wang Z, Westcott J, Toombs JE, et al. AXL is a key factor for cell plasticity and promotes metastasis in Pancreatic cancer. Molecular Cancer Research 2021;19:1412–21. [PubMed: 33811159]
47. Ghiso E, Migliore C, Ciciriello V, Morando E, Petrelli A, Corso S, et al. YAP-Dependent AXL Overexpression Mediates Resistance to EGFR Inhibitors in NSCLC. Neoplasia 2017;19:1012–21. [PubMed: 29136529]
48. Li J, Shi C, Zhou R, Han Y, Xu S, Ma H, et al. The crosstalk between AXL and YAP promotes tumor progression through STAT3 activation in head and neck squamous cell carcinoma. Cancer Sci 2020;111:3222–35. [PubMed: 32589311]
49. Basu S, Totty NF, Irwin MS, Sudol M, Downward J. Akt phosphorylates the Yes-associated protein, YAP, to induce interaction with 14-3-3 and attenuation of p73-mediated apoptosis. Mol Cell 2003;11:11–23. [PubMed: 12535517]

50. Zhang J, Ji JY, Yu M, Overholtzer M, Smolen GA, Wang R, et al. YAP-dependent induction of amphiregulin identifies a non-cell-autonomous component of the Hippo pathway. Nat Cell Biol 2009;11:1444–50. [PubMed: 19935651]
51. Zhang Z, Du J, Wang S, Shao L, Jin K, Li F, et al. OTUB2 Promotes Cancer Metastasis via Hippo-Independent Activation of YAP and TAZ. Mol Cell 2019;73:7–21.e7. [PubMed: 30472188]
52. Hong X, Nguyen HT, Chen Q, Zhang R, Hagman Z, Voorhoeve PM, et al. Opposing activities of the Ras and Hippo pathways converge on regulation of YAP protein turnover. EMBO J 2014;33:2447–57. [PubMed: 25180228]
53. Zhao B, Wei X, Li W, Udan RS, Yang Q, Kim J, et al. Inactivation of YAP oncoprotein by the Hippo pathway is involved in cell contact inhibition and tissue growth control. Genes Dev 2007;21:2747–61. [PubMed: 17974916]
54. Dong J, Feldmann G, Huang J, Wu S, Zhang N, Comerford SA, et al. Elucidation of a Universal Size-Control Mechanism in Drosophila and Mammals. Cell 2007;130:1120–33. [PubMed: 17889654]
55. Rowinsky EK, Windle JJ, Von Hoff DD. Ras protein farnesyltransferase: A strategic target for anticancer therapeutic development. Journal of Clinical Oncology 1999;17:3631–52. [PubMed: 10550163]
56. Kohl NE, Omer CA, Davide JP, Hamilton K, Koblan KS, Kral AM, et al. Inhibition of farnesyltransferase induces regression of mammary and salivary carcinomas in ras transgenic mice. Nature Medicine 1995;1:792–7.
57. End DW, Smets G, Todd AV, Applegate TL, Fuery CJ, Angibaud Patrick, et al. Characterization of the Antitumor Effects of the Selective Farnesyl Protein Transferase Inhibitor R115777 in Vivo and in Vitro. Cancer Res 2001;61:131–7. [PubMed: 11196150]
58. Hanna GJ, Guenette JP, Chau NG, Sayehli CM, Wilhelm C, Metcalf R, et al. Tipifarnib in recurrent, metastatic HRAS-mutant salivary gland cancer. Cancer 2020;126:3972–81. [PubMed: 32557577]
59. Ho AL, Brana I, Haddad R, Bauman J, Bible K, Oosting S, et al. Tipifarnib in head and neck squamous cell carcinoma with HRAS mutations. Journal of Clinical Oncology. 2021;39:1856–64. [PubMed: 33750196]
60. Javaid S, Schaefer A, Goodwin CM, Nguyen VV, Massey FL, Pierobon M, et al. Concurrent Inhibition of ERK and Farnesyltransferase Suppresses the Growth of HRAS Mutant Head and Neck Squamous Cell Carcinoma. Mol Cancer Ther 2022; 21(5):762–774. [PubMed: 35247914]
61. Smith A, Chan S, McCloskey A, Vora H, Burrows F, Malik S. Antitumor Activity of Tipifarnib and PI3K Pathway Inhibitor in HRAS-associated HNSCC. International Journal of Radiation Oncology 2022;112:e48.
62. Zetter BR. Angiogenesis and tumor metastasis. Annu Rev Med 1998;49:407–24. [PubMed: 9509272]
63. Bielenberg DR, Zetter BR. The Contribution of Angiogenesis to the Process of Metastasis. Cancer Journal 2015;21:267–73. [PubMed: 26222078]
64. Micaily I, Johnson J, Argiris A. An update on angiogenesis targeting in head and neck squamous cell carcinoma. Cancers Head Neck 2020;5.
65. Carla C, Daris F, Cecilia B, Francesca B, Francesca C, Paolo F. Angiogenesis in head and neck cancer: A review of the literature. J Oncol 2012;2012: 358472. [PubMed: 22131994]
66. Serban D, Leng J, Cheresh D. H-ras regulates angiogenesis and vascular permeability by activation of distinct downstream effectors. Circ Res 2008;102:1350–8. [PubMed: 18467631]
67. Arbiser JL, Moses MA, Fernandez CA, Ghiso N, Cao Y, Klauber N, et al. Oncogenic H-ras stimulates tumor angiogenesis by two distinct pathways. Proc Natl Acad Sci U S A. 1997;94:861–6. [PubMed: 9023347]
68. Tanaka M, Siemann DW. Axl signaling is an important mediator of tumor angiogenesis. Oncotarget 2019;10:2887–98. [PubMed: 31080559]

Significance of the study:

Mutant HRAS drives metastasis of head and neck cancer by switching off the Hippo pathway to activate the YAP1-AXL axis and stimulate lympho-vascular angiogenesis.

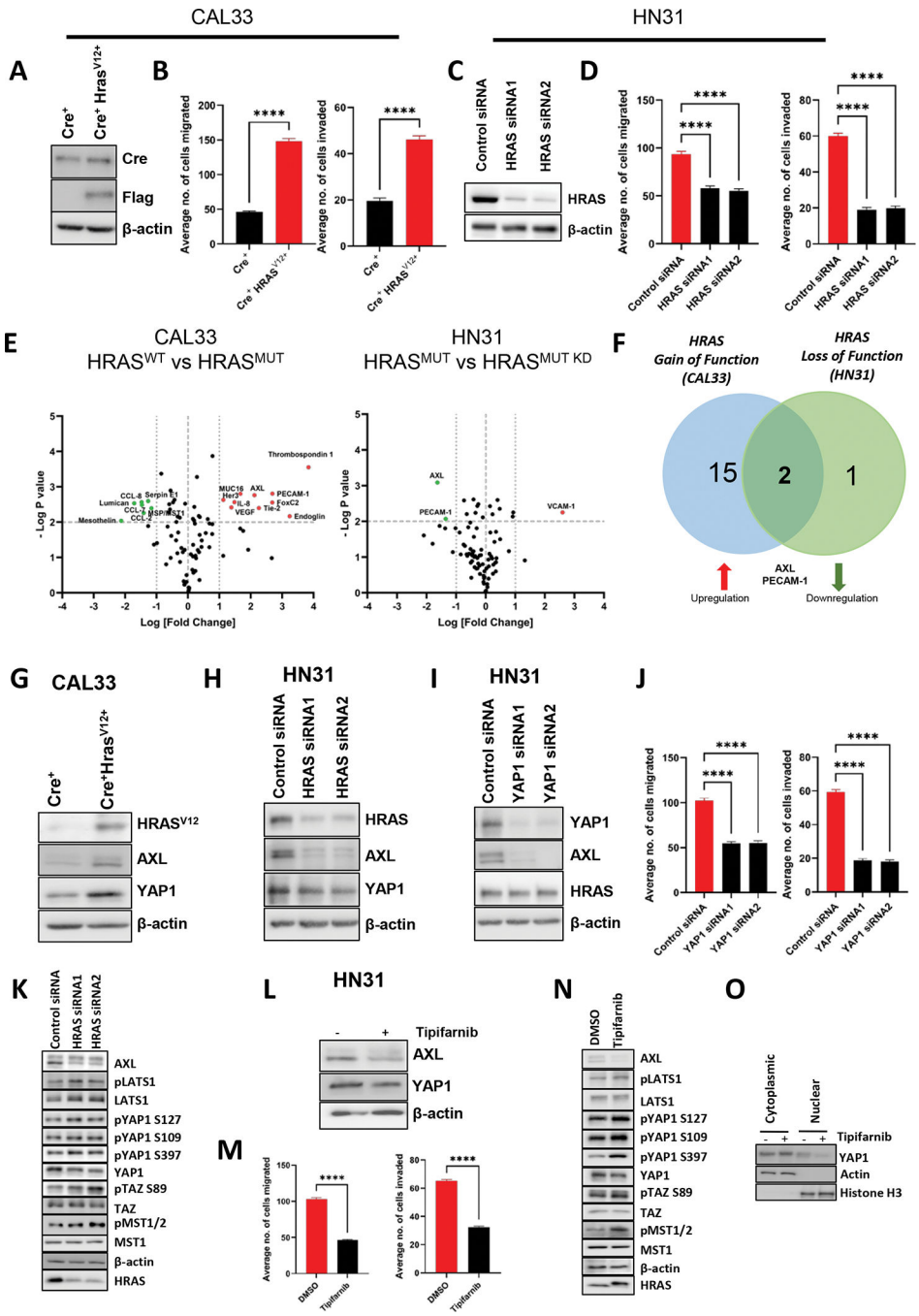

Figure 1: HRAS^{mut} regulates invasive potential *in vitro* via the modulation of AXL through YAP1 activation by switching off Hippo pathway.

A, Western blot confirming the ectopic expression of mutated HRAS^{V12} in the non-metastatic Cre-expressing CAL33 cell line. **B**, Bar graph showing enhanced migration and invasion ability of CAL33 Cre^{+} HRAS^{V12+} cells *in vitro*. **C**, Western blot showing silencing of HRAS expression in an HRAS^{mut} HNC-HN31 cell line. **D**, Silencing of HRAS expression reduces migration and invasive potential of HN31 cells *in vitro*. **E**, Volcanic plot showing the effect of altered expression of oncogenic proteins on HRAS gain of function

(CAL33) and loss of function (HN31). Proteins with a fold change of more than 1 or less than −1 with a P-value less than 0.001 are shown in the plot. **F**, Venn diagram showing proteins altered during gain-of-function and loss-of-function manipulations of HRAS in CAL33 and HN31 cell lines. **G**, Western blot showing effect of enhanced AXL and YAP1 expression on ectopic expression of $HRAS^{V12}$ in CAL33 Cre expressing cells. **H**, Western blot showing effect of AXL and YAP1 downregulation on silencing HRAS expression in HN31 cells. β-actin was used as a loading control. **I**, Western blot confirming YAP1 silencing in HN31 cells with a concomitant reduction in AXL expression. **J**, Bar graph showing that YAP1 silencing also reduces the migration and invasion potential of HN31 cells. **K**, Western blot showing the effect of the expression of various phosphorylated and total proteins in the Hippo pathway, namely, MST1/2, LATS1, YAP1 and TAZ, on silencing HRAS in HN31 cells. **L**, Western blot showing the downregulation of AXL and YAP1 in response to tipifarnib (1 μM) treatment. **M**, Tipifarnib treatment of HN31 cells for 24 h reduces the invasive capability of the cells. **N**, Western blot showing the expression of various phosphorylated and total proteins in the Hippo pathway, namely, MST1, LATS1, YAP1, and TAZ, upon treating HN31 cells with 1 μM tipifarnib for 12 h. **O**, Nuclear and cytoplasmic expression of YAP1 in response to tipifarnib treatment. Actin and histone H3 were used as cytoplasmic and nuclear protein loading controls, respectively. In the different panels of this figure, statistically significant differences (P value = 0.0001) are indicated by ****. Quantification of western blots are provided as supplementary figure 1B, 1C, and 1F–L.

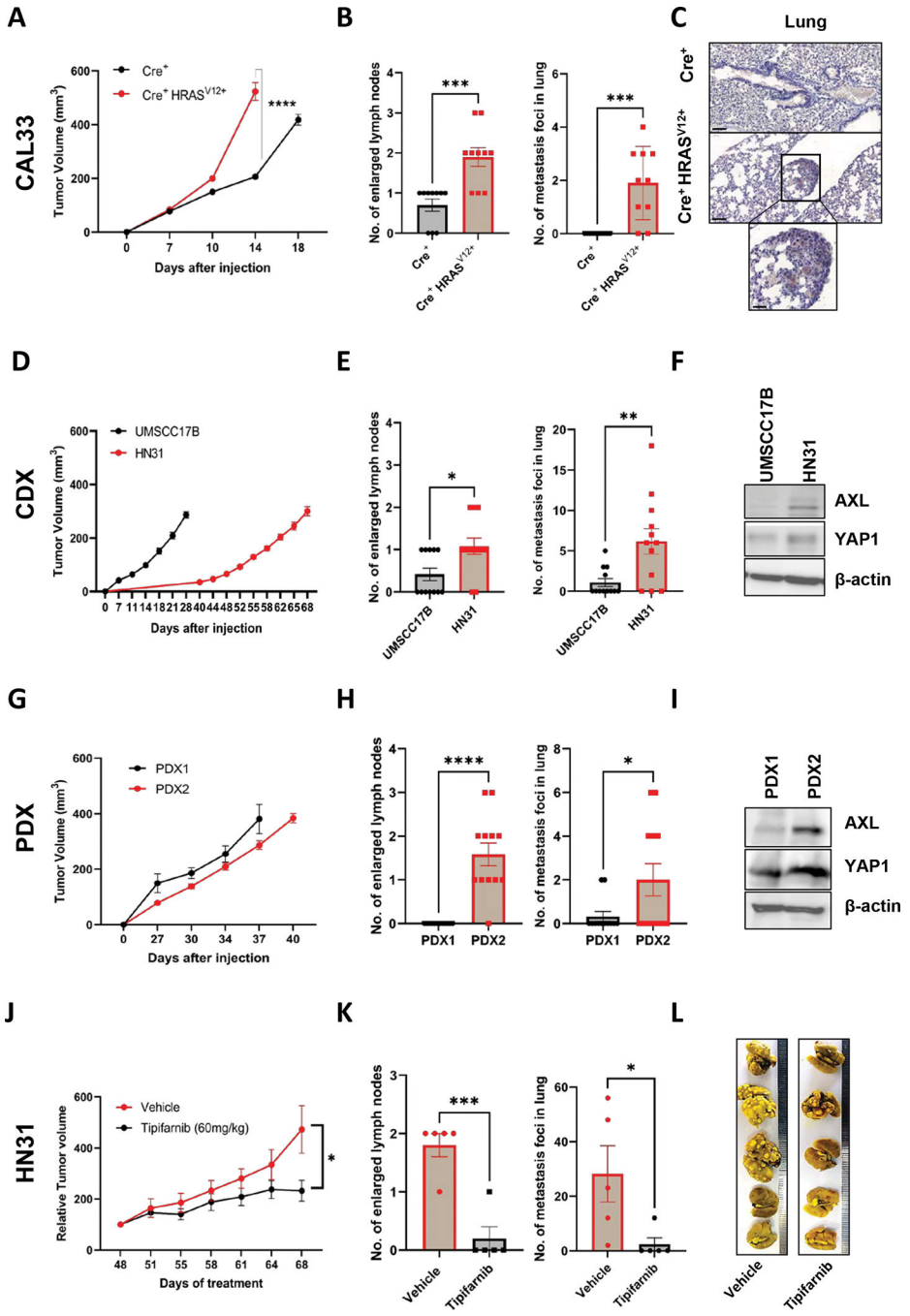

Figure 2: HRAS-YAP1-AXL axis determines the metastatic potential of human HNC cells *in vivo*.

A,B, *In vivo* analysis of (A) tumor growth kinetics and (B) number of enlarged lymph nodes and lung metastasis foci in mice (n = 12) bearing CAL33 Cre^+ or CAL33 Cre^+ $HRAS^{V12+}$ tumors; the figures show the enhanced metastasis potential on the incorporation of HRAS mutation. **C**, Representative immunohistochemistry images of the lung metastases (stained for pan keratin) of CAL33 Cre^+ and CAL33 Cre^+ $HRAS^{V12+}$. Inset magnification 20×. **D, E** *In vivo* analysis of (D) tumor growth kinetics and (E) number of enlarged lymph nodes and

lung metastasis foci in mice (n = 12) injected with $HRAS^{mut}$ HNC cell lines - UMSCC17B or HN31; the figures show the high metastasis potential in HN31 cells. **F,** Western blot showing the expression of AXL and YAP1 in UMSCC17B and HN31 cell lines. β-actin was used as a loading control. **G, H**, *In vivo* representation of (G) tumor growth kinetics, and (H) number of enlarged lymph nodes, and lung metastasis foci in mice (n =12) bearing HRAS mutant HNC PDXs (PDX1 and PDX2) after injection with single cell suspensions into the lip of the NSG mice. **I**, Western blot showing the expression of AXL and YAP1, in PDXs. **J, K**, *In vivo* analysis of (J) relative tumor growth, and (K) the numbers of enlarged lymph nodes and lung metastasis foci in HN31 tumor-bearing mice (n=5–6) treated with tipifarnib (60 mg/kg/twice daily); the findings show a reduced tumor and metastasis burden. **L**, Representative images of lung macro-metastasis; lungs were isolated from vehicle-and tipifarnib-treated HN31 tumor-bearing mice (n=5). In the different panels of this figure, statistically significant differences are indicated by *, **, ***, or **** for P values of 0.05, 0.01, 0.001 or 0.0001, respectively. Quantification of western blots are provided as supplementary figure 2C and 2E.

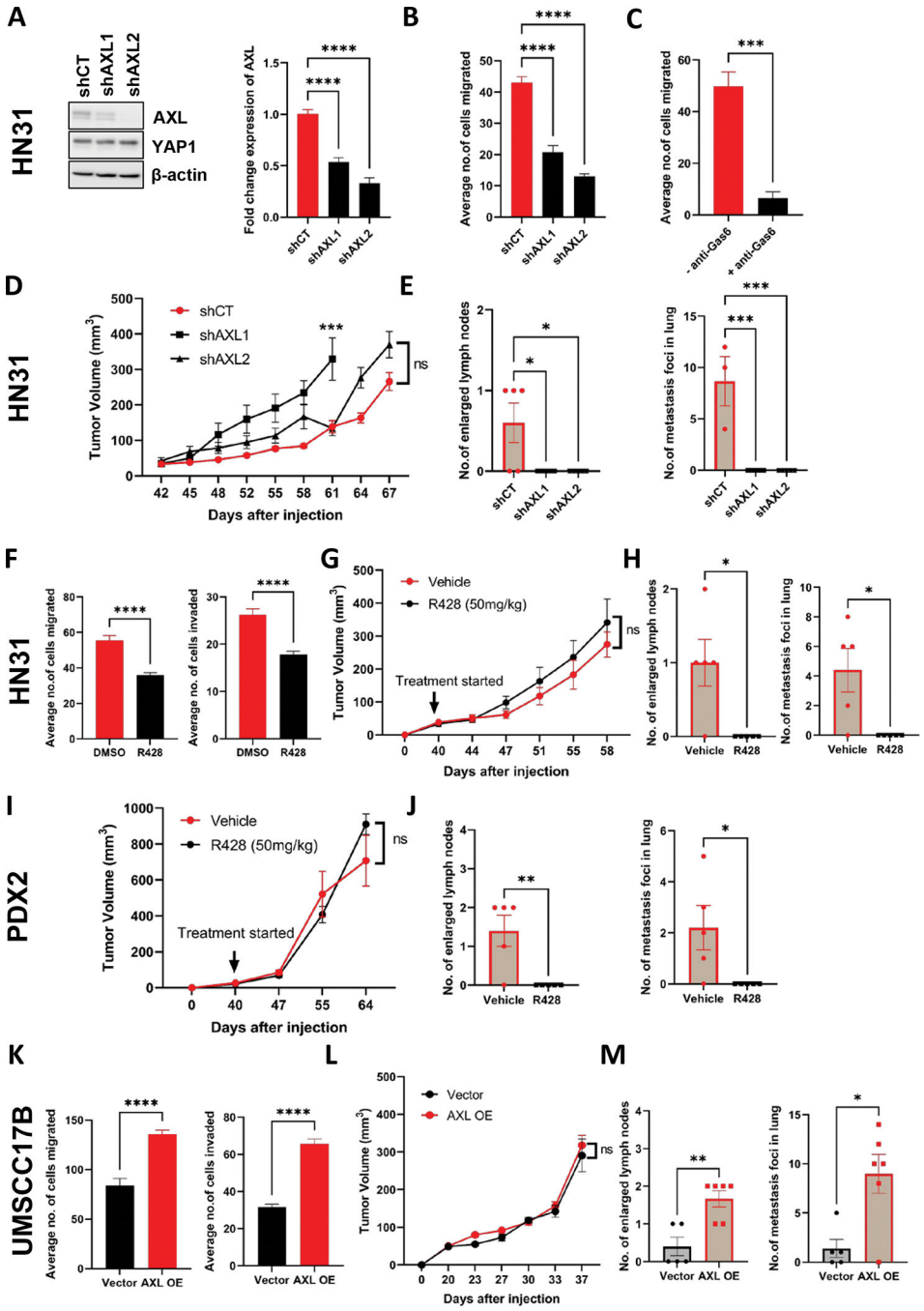

Figure 3: Genetic/pharmacological dysregulation of AXL signaling modulates the metastatic potential of human HRAS^{mut} HNC cells.

A, Western blot and qPCR confirming the AXL knockdown of HN31 cells. **B,** Reduced migration capability of HN31 cells. **C**, Reduced migration capability of HN31 cells upon treatment with anti-Gas6 **D, E,** *In vivo* analysis of (D) tumor growth kinetics and (E) number of enlarged lymph nodes and lung metastasis foci in AXL knockdown HN31 tumor-bearing mice (n = 5). **F**, Bar graphs showing that pharmacological inhibition of AXL signaling by R428 (2 μM) reduces the invasive potential of HN31 cells *in vitro.* **G, H**, *In vivo* analysis

of (G) tumor growth kinetics and (H) number of enlarged lymph nodes and lung metastasis foci in HN31 tumor-bearing mice (n = 5) treated with R428 (50 mg/kg/twice daily). **I,J**, *In vivo* analysis of (I) tumor growth kinetics and (J) number of enlarged lymph nodes and lung metastasis foci (n = 5) in PDX2 tumor-bearing mice treated with R428 (50 mg/kg/twice daily). **K**, AXL overexpression (AXL OE) in weakly metastatic UMSCC17B cell line enhances invasive potential *in vitro* compared to vector control. **L, M**, *In vivo* analysis of (L) tumor growth kinetics and (M) number of enlarged lymph nodes and lung metastasis foci in AXL overexpressing UMSCC17B cells injected mice (n=5). In the different panels of this figure, statistically significant differences are indicated by *, **, ***, or **** for P values of 0.05, 0.01, 0.001 or 0.0001, respectively. ns denotes not significant. Quantification of western blots is provided as supplementary figure 3A.

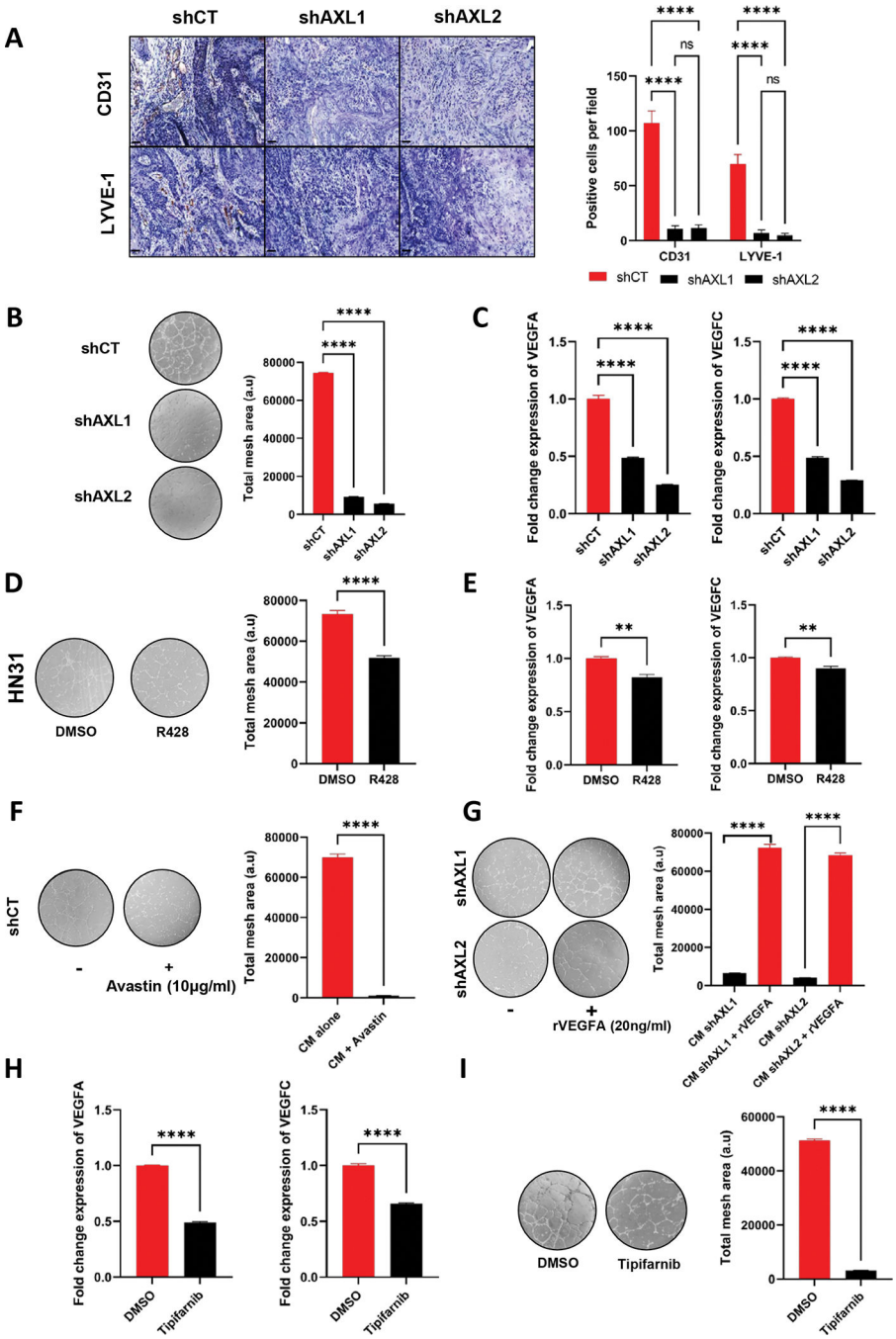

Figure 4: AXL knockdown in HRAS^{mut} HNC attenuates vascular/lymphatic angiogenesis by downregulating VEGFA and VEGFC expression.

A, Immunostaining with CD31 and LYVE-1 (markers for angiogenesis and lymphangiogenesis, respectively) in primary tumors of AXL knockdown HN31; the micrographs show minimal angiogenesis and lymphangiogenesis upon AXL downregulation. The percentage of positive cells per field for each stain is provided on the right. **B**, Representative microscopic images of HUVEC tube formation with conditioned media from AXL knockdown HN31. Bar graphs representing the quantification of total

mesh area on tube formation under each condition are shown on the right. **C**, Fold change in mRNA expression of VEGFA and VEGFC upon AXL knockdown in HN31 cells. **D**, Representative microscopic images of HUVEC tube formation using conditioned media from HN31 cells treated with R428 (2 μM) or DMSO for 24 h. **E**, Fold change in mRNA expression of VEGFA and VEGFC upon treatment of HN31 cells with R428 (2 μM). **F**, **G**, Representative microscopic images of HUVEC tube formation (F) using conditioned media from shCT HN31 cells treated with Avastin (10μg/ml) and (G) in conditioned media from shAXL HN31 cells treated with VEGFA (20ng/ml). Quantification of total mesh area on tube formation under each condition are shown on the right. **H**, Fold change in mRNA expression of VEGFA and VEGFC upon treatment of HN31 cells with tipifarnib (1 μM). **I**, Representative microscopic images of HUVEC tube formation using conditioned media from HN31 cells treated with tipifarnib (1 μM) or DMSO for 24 h. In the different panels of this figure, statistically significant differences ** or **** for P values of 0.01 or 0.0001. ns denotes not significant.

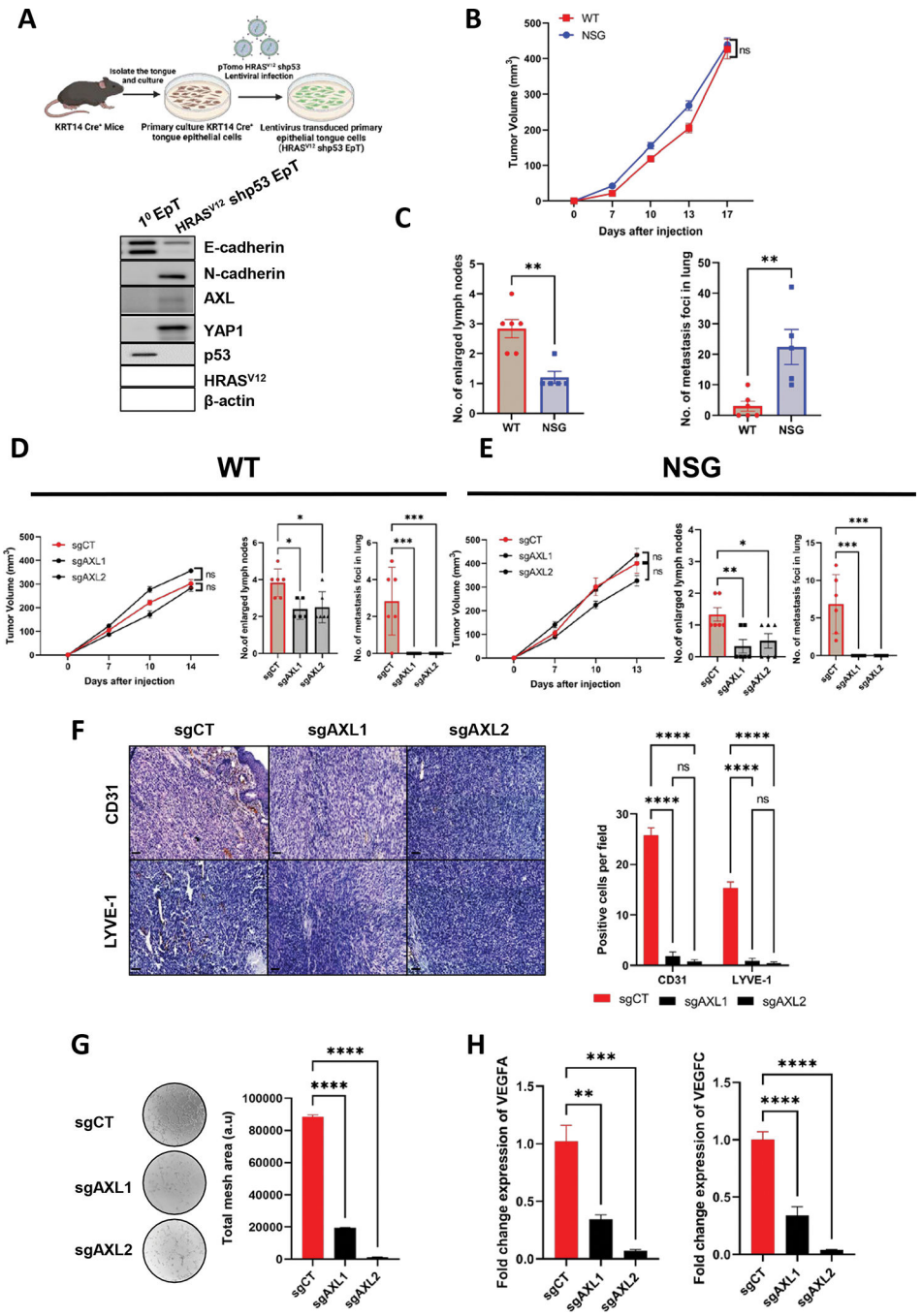

Figure 5: Metastatic potential of murine HRAS^{mut} HNC is modulated by AXL.

A, Top: Schematic representation of the generation of HRAS mutant murine cells from primary KRT14 Cre^{+} tongue epithelial cells. Bottom: Western blot showing the expression of E-cadherin, N-cadherin, AXL, YAP1, p53, HRAS^{V12}, and β-actin in primary tongue epithelial cells (1^{0} EpT) and HRAS^{V12} lentiviral transduced tongue epithelial cells (HRAS^{V12} shp53 EpT). **B, C**, *In vivo* analysis of (B) tumor growth kinetics and (C) number of enlarged lymph nodes and lung metastasis foci of HRAS^{V12} shp53 EpT in WT and NSG mice (n=6). **D, E**, *In vivo* analysis of tumor growth kinetics, number of enlarged lymph

nodes and lung metastasis foci in (D) AXL knockout $HRAS^{V12}$ shp53 EpT tumor-bearing WT mice (n = 6) and (E) AXL knockout $HRAS^{V12}$ shp53 EpT tumor-bearing NSG mice (n = 6) showing a reduced metastatic burden. **F**, Immunostaining with CD31 and LYVE-1 in primary tumors of AXL knockout $HRAS^{V12}$ shp53 EpT showing minimal angiogenesis and lymphangiogenesis upon AXL downregulation. The percentage of positive cells per field for each staining is shown on the right. **G**, Representative microscopic images of HUVEC tube formation with conditioned media from AXL knockout $HRAS^{V12}$ shp53 EpT. Bar graphs representing the quantification of total mesh area on tube formation under each condition are shown on the right. **H**, Fold change in mRNA expression of VEGFA and VEGFC upon AXL knockout in $HRAS^{V12}$ shp53 EpT cells. In the different panels of this figure, statistically significant differences are indicated by **, ***, or **** for P values of 0.01, 0.001 or 0.0001, respectively. ns denotes not significant. Quantification of western blots are provided as supplementary figure 5D.

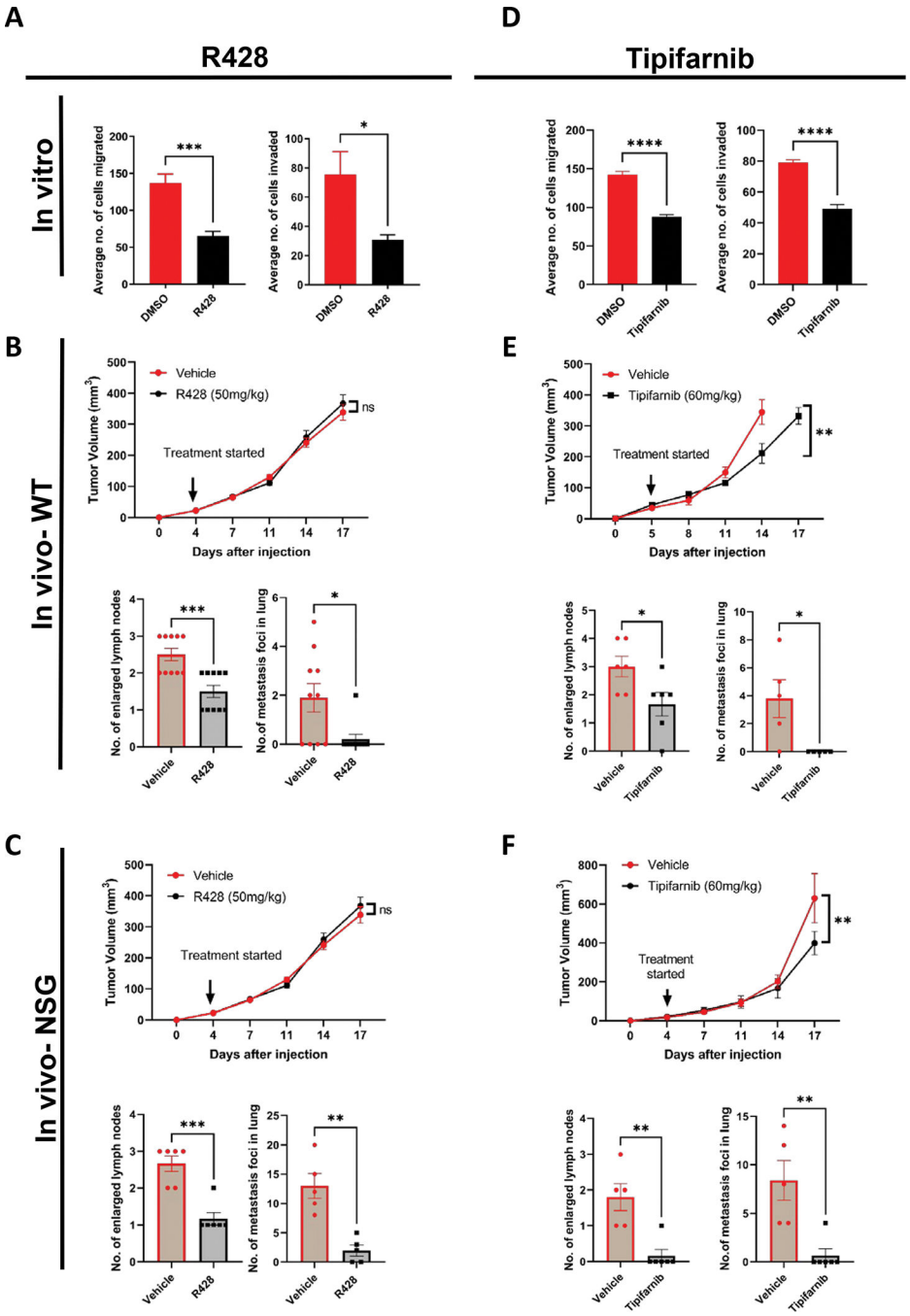

Figure 6: Inhibition of HRAS/AXL signaling diminishes the metastatic potential of murine HRAS^{mut} cells.

A, Pharmacological inhibition of AXL signaling with R428 reduced the migration and invasion of HRAS^{V12} shp53 EpT. **B, C**, *In vivo* analysis of tumor growth kinetics, and numbers of enlarged lymph nodes and lung metastasis foci in HRAS^{V12} shp53 EpT tumor upon treatment with R428 (50 mg/kg/twice daily) in (B) WT mice (n=5) and (C) NSG mice (n=5), showing R428 treatment reduced the metastatic burden without affecting the tumor growth in both WT and NSG mice. **D**, Pharmacological inhibition of HRAS signaling with

tipifarnib reduced the migration and invasion of $HRAS^{V12}$ shp53 EpT. **E, F**, *In vivo* analysis of tumor growth kinetics, and numbers of enlarged lymph nodes and lung metastasis foci in $HRAS^{V12}$ shp53 EpT tumor-baering WT (E) and NSG (F) mice (n = 6) treated with tipifarnib (60 mg/kg/twice daily) showing tumor growth delay and reduced metastatic burden in both WT and NSG mice. In the different panels of this figure, statistically significant differences are indicated by **, ***, or **** for P values of 0.01, 0.001 or 0.0001, respectively. ns denotes not significant.

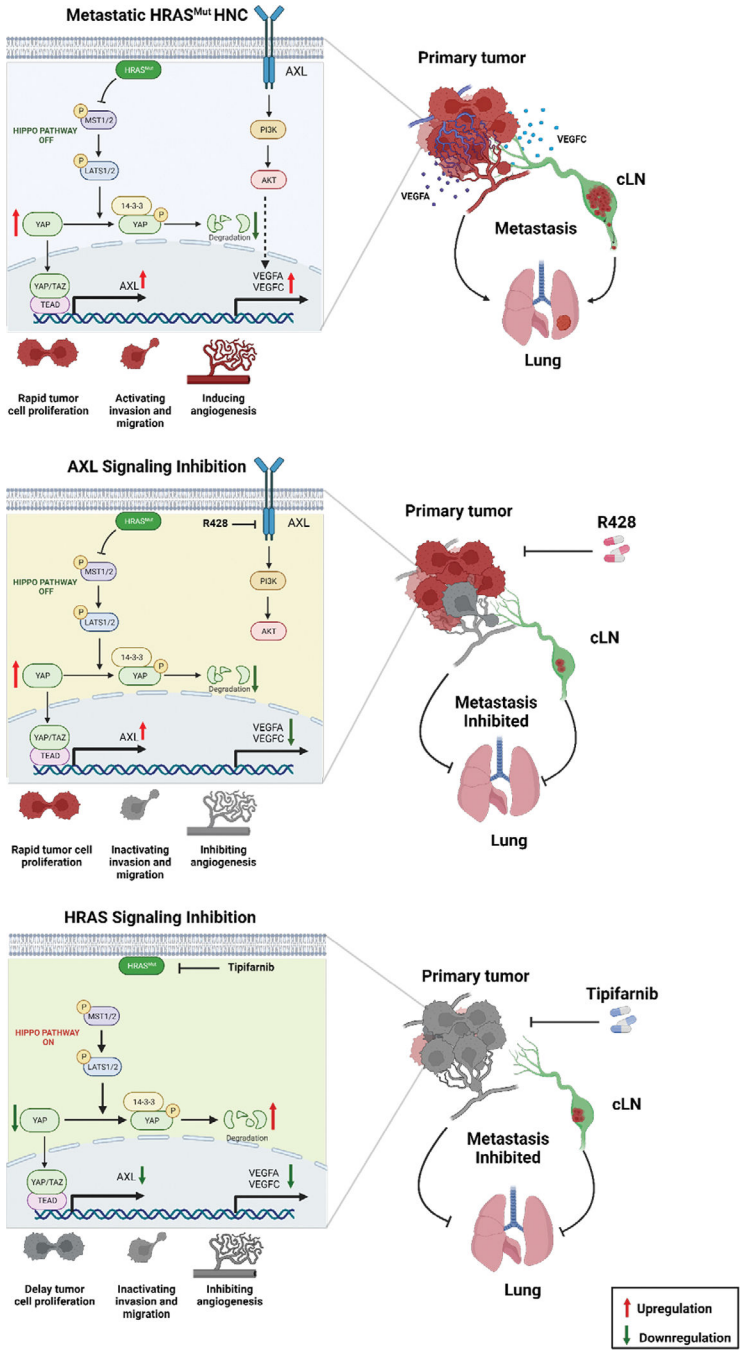

Figure 7: Schematic representation of the molecular mechanism of HRAS-mutation-mediated metastasis in HNC.

Top - In the disease state, HRAS^{mut} inhibits the Hippo pathway, preventing YAP1 degradation and, in turn, leading to nuclear export of YAP1, thereby regulating the transcriptional expression of multiple genes, including AXL. AXL overexpression and activation by its ligand Gas6 enhance the migratory activity of tumor cells and upregulate the expression of VEGFA, VEGFC and other angiogenic factors as well as EMT genes. This activation of HRAS-YAP1-AXL enhanced angiogenesis, sustained proliferation, and

increased metastasis potential, causing metastatic spread to the cLNs and lungs. **Middle** - Treament of tumors with R428 did not reduce tumor cell proliferation but did reduce the metastasis potential of tumor cells and tumor angiogenesis by down-regulating angiogenic factors as well as reversing the EMT, leading to diminished metastatic spread to the cLNs and lungs. **Bottom** - Treament of tumors with tipifarnib blocked the activation of HRAS, thus switching off the Hippo pathway and causing YAP1 degradation and down-regulation of AXL expression. This deactivation of HRAS-YAP1-AXL reduced the proliferation and metastasis potential of tumor cells and tumor angiogenesis, leading to diminished metastatic spread to the cLNs and lungs. (This scheme is created with BioRender.com)